Chin. J. Astron. Astrophys. Vol. 6 (2006), **Suppl. 1**, 119–124
(*http://www.chjaa.org*)

Chinese Journal of
Astronomy and
Astrophysics

# *Chandra* Observations of the $\rho$ Ophiuchi Cloud

Katsuji Koyama ⋆ and Kensuke Imanishi

Department of Physics, Kyoto University, Kita-Shirakawa, Sakyo-ku, Kyoto, 606-8502, Japan

**Abstract** $Chandra$ observed two regions near the cores of the $\rho$ Ophiuchi dark cloud. A 100-ks exposure for each observation revealed $\sim$ 200 X-ray sources above the detection limit of $\sim 10^{28}$ erg s$^{-1}$. About 60% (110) are identified with an optical and/or infrared counterpart, including significant numbers of Class I sources and brown dwarfs. Three Class 0 candidates are newly discovered with the X-rays. Many X-ray flares, possibly due to the magnetic activity, are found from all of the Classes. We report the results of the systematic spectral and timing analysis on the quiescent and flare X-rays.

**Key words:** X-rays: young stars – stars: Pre-main sequence – stars: individual ($\rho$ Ophiuchi dark cloud)

## 1 INTRODUCTION

The $\rho$ Ophiuchi molecular cloud ($\rho$ Oph) is one of the nearest star forming region of 165 pc distance containing many low mass young stellar objects (YSOs) in various mass and age ranges. (Dame et al. 1987). These low-mass YSOs have been classified by the infrared - sub $mm$ radio spectral energy distributions (SEDs). The youngest is protostar, which is deeply embedded in molecular cloud cores and is represented by Class 0 or Class I SEDs, depending on the evolutional stages. Then followed by Class II and Class III SEDs, which are respectively called Classical T Tauri Stars (CTTSs) and Weak-line T Tauri Stars (WTTSs).

With the *Einstein* satellite, T Tauri stars (TTSs = CTTSs and WTTSs) in $\rho$ Oph have been found to emit fairly strong soft X-rays, with the plasma temperature of $\sim$ 1 keV and rapid time variability like solar flares (Montmerle et al. 1983). These are consistent with the scenario of enhanced solar–type activity, attributable to magnetic dynamo processes.

Since protostars (Class 0 and Class I) are embedded deeply in star forming clouds and shrouded by dense circumstellar gas and dust, they are generally invisible in the optical, near infrared or even soft X-ray bands. X-rays from Class Is (the late phase of protostars) in $\rho$ Oph are discovered in the hard X-ray band ($>$ 2 keV) with the $ASCA$ satellite (Koyama et al. 1994). However possible contamination from nearby TTSs (or others) would not be removed with the limited spatial resolution of *ASCA*. In order to shed light on the embedded YSOs, like Class I sources in $\rho$ Oph , deep exposure observations on this cloud were made with the *Chandra X-ray Observatory*. The observations inevitably provide an excellent sample of X-ray emissions from low mass YSOs, hence enable us to do systematic study of X-ray emissions from these YSOs. This paper presents the results and discussions based on these observations. More details are given in Imanishi et al. 2003, 2001a, 2001b. The source names (abbreviations) used in this paper are adopted after Greene & Young 1992 (GY), Wilking & Lada 1983 (WL), and Young, Lada & Wilking 1986 (YLW).

## 2 DETECTION OF X-RAYS FROM CLASS I

The $\rho$ Oph molecular cloud has many cores as is given by the 1.3 mm radio map (Figure 1; left) . $Chandra$ pointed two major parts, namely on core A and on cores B, C, E, and F. A mosaic X-ray map of 100-ks exposure each is given in Figure 1 (right). From this region, we detected about 200 X-ray sources above the detection limit of $10^{28}$ erg s$^{-1}$. About 60% (110) of the X-ray sources are identified with an optical and/or infrared counterpart. In this field, $\sim$15 Class Is have been reported with near- to far-IR observations.

⋆ E-mail: koyama@cr.scphys.kyoto-u.ac.jp

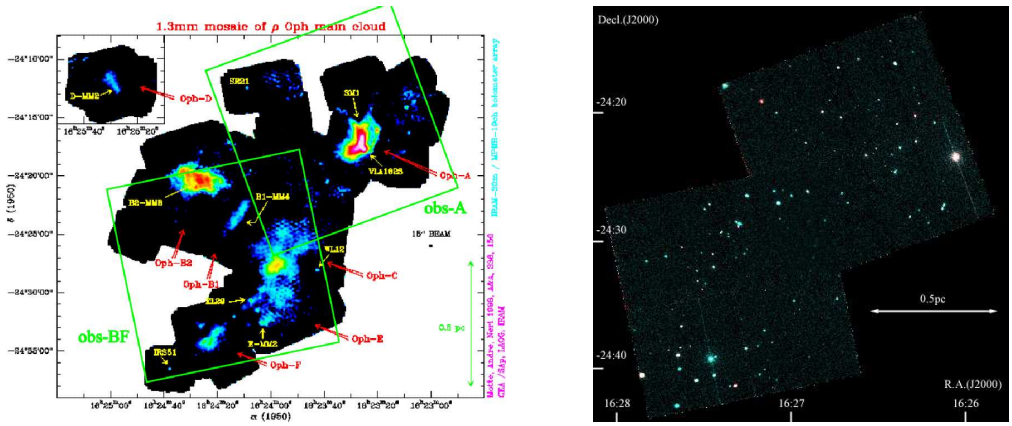


**Fig. 1** (Left) The radio 1.3 mm emission from the cores of $\rho$ Oph (Motte et al 1998). The two squares are the field of view of the *Chandra* observations. (Right) A mosaic ACIS-I image of $\rho$ Oph. Red and blue colors represent photons in the soft (0.7–2.0 keV) and hard (2.0–7.0 keV) X-ray bands, respectively (after Imanishi 2003, PhD Thesis, Kyoto University).

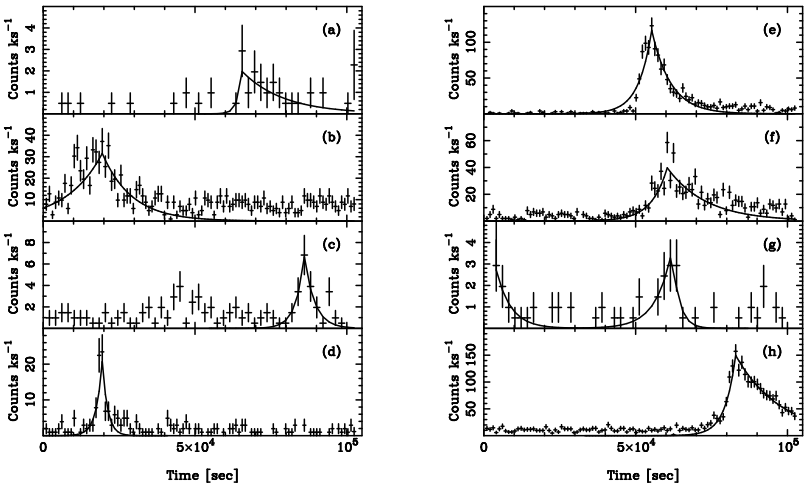


**Fig. 2** Light curves of the Class Is in the 0.7–7.0 keV band. The horizontal axis is the time from the observation start (MJD = 51647.77). The best-fit exponential models for the rise and decay phases are shown by the solid lines. (a): WL 21; (b): EL 29; (c): GY 224; (d): WL 19; (e): YLW 10; (f): WL 20; (g): GY 256; (h): YLW 15A (after Imanishi et al. 2001a).

About half of them ($\sim 50\%$) are found to emit X-ray. The X-ray spectra are fitted with a thin thermal plasma model in the temperature rage of $\sim$ 1–10 keV, similar to, but systematically higher than those of Class II-IIIs (see Section 5). All the Class Is show short time variability as are given in Figure 2. The non-detection of X-rays from the other Class Is could be partly due to the short time variability. For example, WL21 (Figure 2-a) can be hardly visible in its quiescent phase. Also, long-term variability, like the 11-year cycle of solar activity, may not be ignored. We hence suspect that all the Class Is, at least those in $\rho$ Oph, are potential X-ray sources.

A Class I source YLW16A exhibited a giant flare. The spectrum is fitted with a thin thermal plasma of $\sim$10 keV temperature. A remarkable finding is an additional emission line feature near the 6.7 keV line

from the high temperature plasma (highly ionized iron). The best-fit line energy is $6.4^{+0.1}_{-0.4}$ keV, which is attributable to neutral or low ionized iron. The most plausible origin is fluorescence from cold iron in the circumstellar gas. If the circumstellar gas is spherically distributed around the X-ray source, the equivalent width of iron is estimated to be $\approx 10 Z_{\rm Fe}(N_{\rm H}/10^{22}$ cm$^{-2})$ eV, where $Z_{\rm Fe}$ and $N_{\rm H}$ are the abundance of iron and column density, respectively (Inoue 1985). Using the observed column density of $4.7\times10^{22}$ cm$^{-3}$ and the mean iron abundance of 0.3 solar, we can predict the equivalent width to be ≈15 eV. This is significantly lower than the observed value of ≈100 eV, hence requires non-spherical geometry; a larger amount of gas should be present out of the line-of-sight. A possible scenario is that YLW 16A has a disk of face-on geometry (Sekimoto et al. 1997) looking the flare with large opening angle. Since we see no time-lag (reflection time scale) between the flare on-set and the 6.4 keV iron line appearance within $< 10^4$ s, the separation between the star and the reflector should be less than 20 AU, consistent with that the reflector is the accretion disk.

## 3 X-RAYS OF BROWN DWARFS

We detected X-ray emissions of $\sim$ 30% BDs from 18 IR detected BDs in $\rho$ Oph (Barsony et al. 1997). To investigate the origin of the X-rays, we compared the bolometric ($L_{\rm bol}$) and X-ray ($L_{\rm X}$) luminosities. $L_{\rm bol}$ is roughly proportional to the area of the photosphere, hence $L_{\rm X}/L_{\rm bol}$ is a good indicator of coronal X-ray activity per unit surface area. The $L_{\rm X}/L_{\rm bol}$ value lies between $10^{-3}$–$10^{-5}$, which is similar to low-mass pre-main-sequence stars (e.g., Imanishi et al. 2001a).

It should also be noted that most of the upper limits of $L_{\rm X}/L_{\rm bol}$ for X-ray non-detected BDs are scattered around $10^{-3}$–$10^{-5}$, which are comparable with or slightly lower than those of X-ray detected BDs. This leads us to suspect that the X-ray non-detected BDs may emit X-rays slightly below the sensitivity limit of the current *Chandra* observations.

We also obtain the X-ray spectra from the BDs for the first time , which are fitted with a thin thermal plasma model of $\sim$ 1-2 keV temperature. Solar-like flares are also detected from 2 BDs (GY 31 and GY 59). These X-ray features are similar to those of low-mass stars. Together with the high $L_{\rm X}/L_{\rm bol}$ value, we suggest that X-rays from BDs are attributable to magnetic activities like low–mass stars.

One debatable issue is the mechanism of magnetic field amplification. Brown dwarfs and protostars are fully convective, hence the standard dynamo ($\alpha$-$\omega$ dynamo) mechanism may not work. As one possible scenario, Montmerle et al. 2000 proposed magnetic loops connecting the star and the circumstellar disk. The magnetic amplification and reconnection is due to twisting through the differential rotation between star and disk.

## 4 CLASS 0 CANDIDATES IN THE CLOUD CORES

Most of the unidentified X-ray sources would be background AGNs. However some fractions would be either BDs, Class Is, or Class 0s. To search for such candidates. We searched for the unidentified X-ray sources (no IR counterpart of limiting K-magnitude of $K > 15$ from Barsony et al. 1997 ) in the cloud core clumps, and three candidates A–29, A–31 and A–36 are found at the respective positions of $(\alpha, \delta)_{2000}$ = $(16^{\rm h}26^{\rm m}27^{\rm s}.47, -24^\circ24'17''.8)$, $(16^{\rm h}26^{\rm m}27^{\rm s}.89, -24^\circ23'59''.2)$ and $(16^{\rm h}27^{\rm m}16^{\rm s}.41, -24^\circ31'14''.7)$. Figure 5 shows two of them (A–29, A–31) in the dense core shown by the 1.3-mm contours (Motte et al. 1998). All the three sources show flare-like time variability (see Figure 4), resembling those of TTS or protostars. The absorption of A-29 and A-31 are $2.5 \times 10^{23}$ and $5.4 \times 10^{23}$, respectively, which are significantly larger than Class Is (mean value is $7 \times 10^{22}$ ), and more likely to those of Class 0 candidates in the OMC 2 and 3 clouds ($1 - 3 \times 10^{23}$: Tsuboi et al. 2001), and that in the R Cor A dark cloud ($3 \times 10^{23}$: Hamaguchi et al. 2005). Thus our new sources would be younger than Class I and likely to be Class 0s.

## 5 COMPARISON BETWEEN CLASS I, II AND IIIs

From all the Class I–III sources, we have detected more than 50 X-ray flares. We summarize the X-ray properties of the quiescent and flare phases. In Figure 5, we show the luminosity functions of Class I , II and IIIs. The mean luminosities (in the unit of erg s$^{-1}$) in quiescent are log[$L_{\rm X}$]= $29.8 \pm 0.2$, $29.5 \pm 0.1$ and $29.5 \pm 0.1$, for Class I, II and IIIs, while those in flare are $30.9 \pm 0.2$, $30.4 \pm 0.1$, $30.5 \pm 0.2$. Thus we conclude that:

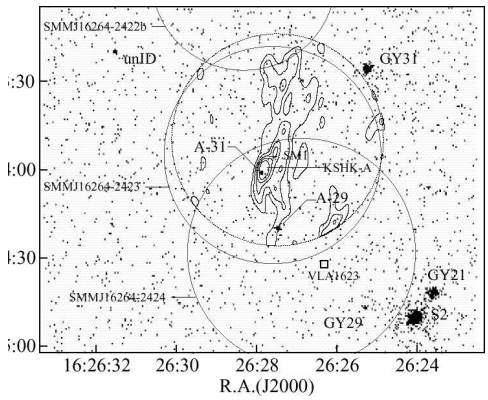


**Fig. 3** The X-ray image around the 1.3-mm cores SM1 in the 2.0–9.0 keV band overlaid on the 1.3-mm contours (Motte et al. 1998). Solid and dotted circles are the size of 850-$\mu$ clumps (Johnstone et al. 2000) and fi eld of view of the 1.3-mm observation, respectively. The square is the position of the Class 0 sources VLA 1623. GY 31 is a brown dwarf. Two X-ray sources (A-29 and A-31) with no IR Counterpart are found at the cloud core (after Imanishi 2003, PhD Thesis, Kyoto University).

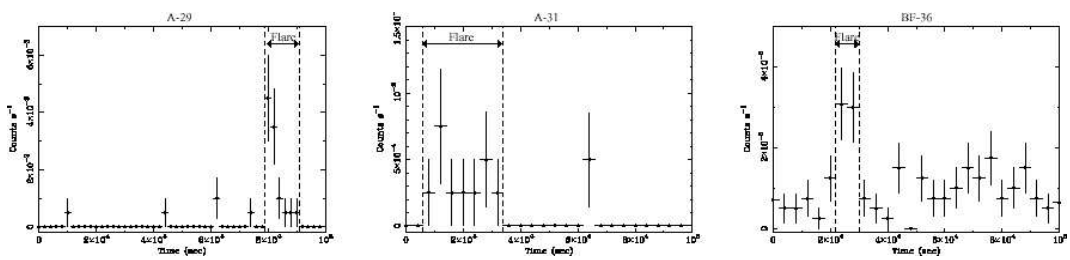


**Fig. 4** Light Curves of the three Class 0 candidates, A-29, A-31 and BF-36 (from left to right). The time bins are 2000 sec (A-29) and 4000 sec (A-31 and BF-36) (after Imanishi 2003, PhD Thesis, Kyoto University).

(1) The X-ray luminosity of Class Is is systematically higher than those of Class II–IIIs, both in quiescent and flare.

The distributions of the mean X-ray temperature $\langle kT \rangle$ are separately given in Figure 6, for Class I, II and III (from top to down), and for quiescent (left) and flare (right). The mean temperatures in quiescent are $\langle kT \rangle$ = $2.9 \pm 0.3$, $2.3 \pm 0.2$ keV and $1.7 \pm 0.1$ keV, for Class I, II and IIIs, while those in flare are $5.2 \pm 0.9$, $3.9 \pm 0.4$, $2.7 \pm 0.2$ keV.

(2) The mean temperatures in quiescent and flare decrease along the evolutional phase such that Class I is the highest and Class III is the lowest. The flare temperature sometimes becomes as high as 10 keV.

## 6 FLARE PROFILE ANALYSIS

Most of the YSO flares have the typical profiles of a fast rise and slow decay (see Fig. 2). We derived the time-averaged temperature $\langle kT \rangle$, luminosity $\langle L_{\rm X} \rangle$, rise and decay timescales ($\tau_{\rm r}$ and $\tau_{\rm d}$) of the flares. Then we made a simple estimation to derive the flare parameters based on the magnetic reconnection model. The observational parameters are the exponential rise and decay times ( $\tau_{\rm r}$ and $\tau_{\rm d}$ ) of the flares (see Fig. 2 for Class Is) and the mean flare temperature $\langle kT \rangle$. The physical parameters to be derived are the pre-flare (coronal) density ($n$), the half-length of the magnetic loop ($L$), and the magnetic field strength ($B$).

Basic assumptions in our model are:

(1) The flare temperature is determined by the balance of heating rate (magnetic reconnection) and conduction cooling rate.

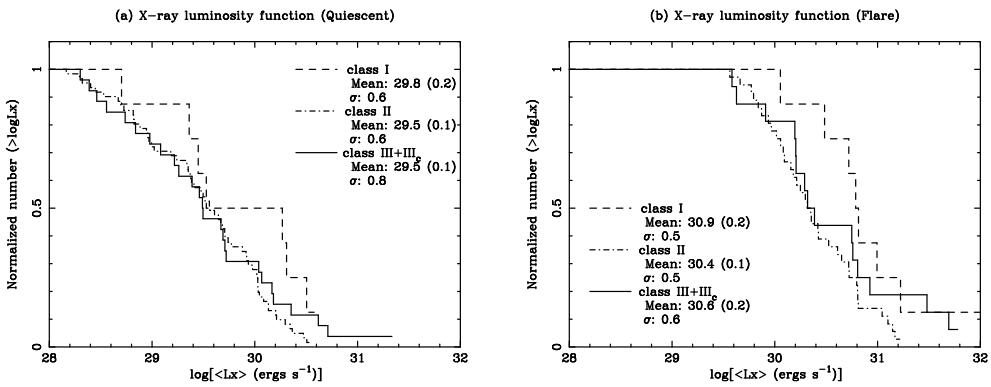


**Fig. 5** Normalized X-ray luminosity functions of Class I (dashed), Class II (dash–dotted), and Class III (solid) sources in the (left) quiescent and (right) flare phases. The mean value (Mean) and standard deviation ($\sigma$) of log[$L_{\rm X}$] in the unit of erg s$^{-1}$ for each Class are shown in the figures. The parentheses indicate errors of the mean values (after Imanishi et al. 2003).

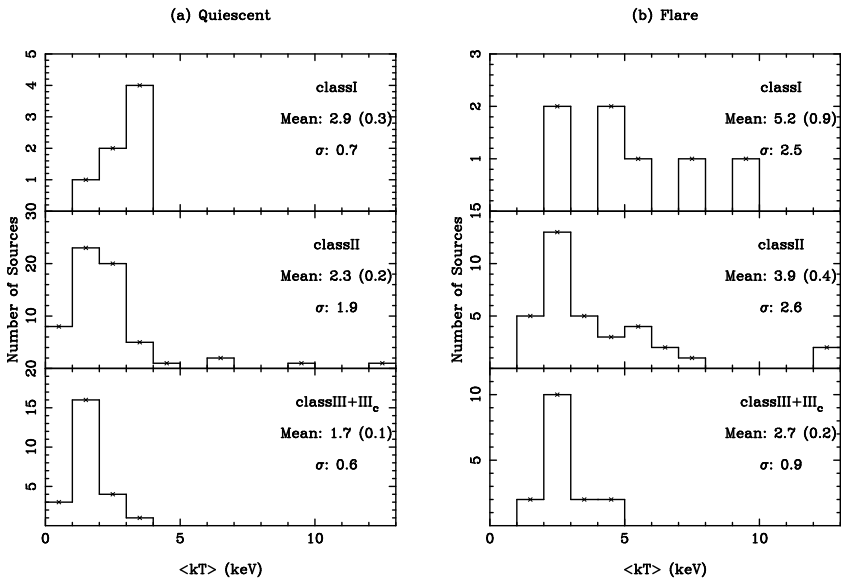


**Fig. 6** Histograms of $kT$ in the quiescent (left), and flare phases (right) for each class, with their mean values (Mean) and standard deviation ($\sigma$) in the unit of keV for each class. The parentheses indicate errors of the mean values (after Imanishi et al. 2003).

(2) The rise time of the flare is proportional to the loop length divided by the Alfven velocity.
(3) The decay time of the flare is equal to the radiative cooling time.
(4) The magnetic pressure at the flare peak is equal to the plasma pressure.
The details of the formulations are given in Imanishi et al. 2003. Here we summarize the results.

$$\frac{\tau_{\rm d}}{\rm s} = A\left(\frac{\tau_{\rm r}}{\rm s}\right)^{1/2}, \tag{1}$$

where constant A is a function of density ($n$), and can be determined by the observational results of $\tau_{\rm r}$ and $\tau_{\rm d}$ relation shown in Figure 7 (left). The solid line represents the best-fit log-linear correlation, while the

dashed-dotted line is the best-fit of Equation 1. Good agreement with each other is found, which supports the reality of this model. Using the best-fit density ($n = 10^{10.48}$ cm$^{-3}$), we can drive the rise time $\tau_{\rm r}$ as a function of ($B$, $\langle kT \rangle$) or ($L$, $\langle kT \rangle$) as follows:

$$\tau_{\rm r} \cong 10^{3.68} \left( \frac{B}{100\ {\rm G}} \right)^{-4} \left( \frac{\langle kT \rangle}{\rm keV} \right)^{7/2} \ [{\rm s}], \tag{2}$$

$$\tau_{\rm r} \cong 10^{5.31} \left( \frac{L}{10^{11}\ {\rm cm}} \right)^{4/3} \left( \frac{\langle kT \rangle}{\rm keV} \right)^{-7/6} \ [{\rm s}]. \tag{3}$$

From Figure 7 (right), the loop lengths are estimated to be $10^{10} - 10^{11}$ cm, which are comparable to the typical stellar radius of low mass YSOs. The higher $\langle kT \rangle$ observed for Class Is may be explained by a slightly higher magnetic field strength ($\approx$ 500 G) than for Class II–IIIs (200–300 G).

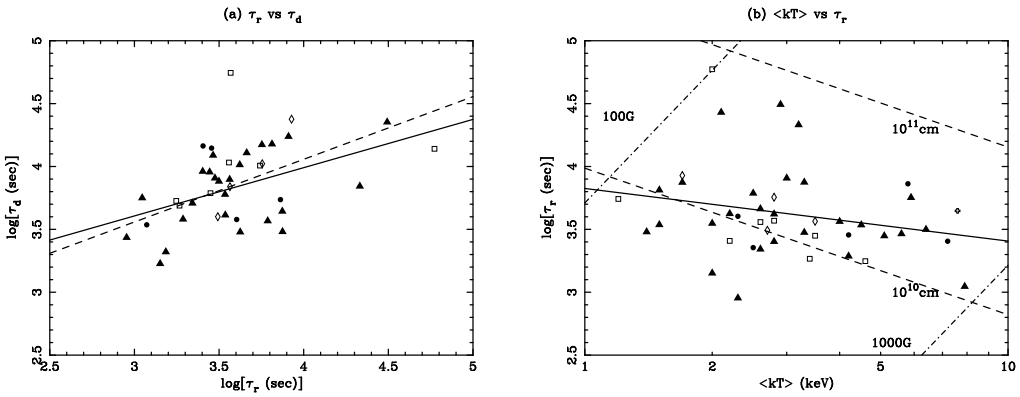


**Fig. 7** Relations between (left) $\tau_{\rm r}$ $vs$ $\tau_{\rm d}$ and (right) $kT$ $vs$ $\tau_{\rm r}$. The circles, triangles, squares, diamonds, and crosses represent fhres from Class I, Class II, Class IIIs, unclassifi ed NIR sources, and unidentifi ed sources, respectively. The solid lines represent the best-fi t log-linear correlations. The dashed line in (a) is the best-fi t model of Equation (1), while the dash-dotted and dashed lines in (b) are constant $B$ and $L$ lines derived by Equations (2) and (3) with the assumption of $n$ = $10^{10.48}$ cm$^{-3}$ (after Imanishi et al. 2003).

## References

Barsony, M. K., Scott, J., Lada, E. A., Teuben, P. J. 1997, ApJS, 112, 109
Dame, T. M., Ungerechts, H., Cohen, R. S., de Geus, E. J., Grenier, I. A., May, J., Murphy, D. C., Nyman, L.-A., Thaddeus, P. 1987, ApJ, 322, 706
Greene, T. P., Young, E. T. 1992, ApJ, 395, 516
Hamaguchi, K., Corcoran, M. F., Petre, R., White, N. E., Stelzer, B., Nedachi, K., Kobayashi, N. , Tokunaga, A. T. 2005, ApJ, 623, 291
Imanishi, K., Koyama, K., Tsuboi, Y. 2001a, ApJ, 557, 747
Imanishi, K., Tsujimoto, M., Koyama, K. 2001b, ApJ, 563, 361
Imanishi, K., Nakajima, H., Tsujimoto, M., Koyama, K., Tsuboi, Y. 2003, PASJ, 55, 653
Inoue, H. 1985, Space Sci. Rev., 40, 317
Johnstone, D., Wilson, C. D., Moriarty-Schieven, G., Joncas, G., Smitt, G. Gregersen, E. Fich, M. 2000, ApJ, 545, 327
Koyama, K., Maeda, Y., Ozaki, M., Ueno, S., Kamata, Y., Tawara, Y., Skinner, S., Yamauchi, S. 1994, PASJ, 46, L125
Montmerle, T., Koch-Miramond, L., Falgarone, E., Grindlay, J. E. 1983, ApJ, 269, 182
Montmerle, T., Grosso, N., Tsuboi, Y., Koyama, K. 2000, ApJ, 532, 1097
Motte, F., Andre, P., Neri, R., 1998, A&A, 336, 150
Sekimoto, Y., Tatematsu, K., Umemoto, T., Koyama, K., Tsuboi, Y. Hirano, N., Yamamoto, S. 1997, ApJ, 489, 63
Tsuboi,Y., Koyama,K., Hamaguchi, K., Tatematsu, K., Sekimoto, Y., Bally, J., Reipurth, B. 2001, ApJ, 554, 734
Wilking, B. A., Lada, C. J. 1983, ApJ, 274, 698
Young, E. T., Lada, C. J., Wilking, B. A. 1986, ApJ, 304, L45